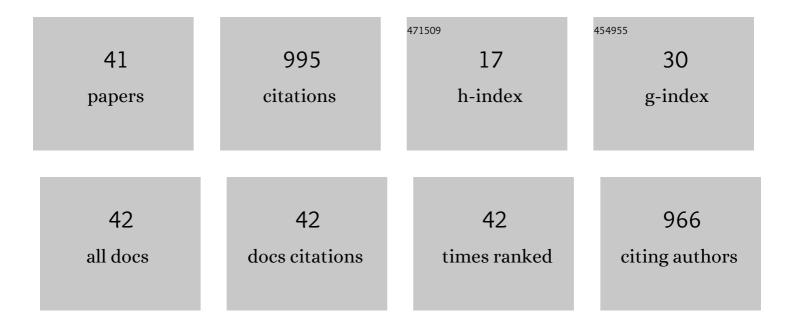
Wanpeng Feng

List of Publications by Year in descending order

Source: https://exaly.com/author-pdf/389136/publications.pdf Version: 2024-02-01



WANDENC FENC

#	Article	IF	CITATIONS
1	InSAR data reveal that the largest hydraulic fracturing-induced earthquake in Canada, to date, is a slow-slip event. Scientific Reports, 2022, 12, 2043.	3.3	26
2	Supershear Rupture During the 2021 <i>M</i> _W 7.4 Maduo, China, Earthquake. Geophysical Research Letters, 2022, 49, .	4.0	22
3	Source Characteristics and Exacerbated Tsunami Hazard of the 2020 Mw 6.9 Samos Earthquake in Eastern Aegean Sea. Journal of Geophysical Research: Solid Earth, 2022, 127, .	3.4	7
4	Mechanism of the 2017 <i>M</i> w 6.3 Pasni earthquake and its significance for future major earthquakes in the eastern Makran. Geophysical Journal International, 2022, 231, 1434-1445.	2.4	3
5	Reconstruction and Evaluation of DEMs From Bistatic Tandem-X SAR in Mountainous and Coastal Areas of China. IEEE Journal of Selected Topics in Applied Earth Observations and Remote Sensing, 2021, 14, 5152-5170.	4.9	7
6	Topography-correlated atmospheric signal mitigation for InSAR applications in the Tibetan plateau based on global atmospheric models. International Journal of Remote Sensing, 2021, 42, 4361-4379.	2.9	11
7	Confirmation and Characterization of the Rupture Model of the 2017 MsÂ7.0 Jiuzhaigou, China, Earthquake. Seismological Research Letters, 2021, 92, 2927-2942.	1.9	5
8	Diverse rupture processes of the 2014 Kangding, China, earthquake doublet (MW 6.0 and 5.7) and driving mechanisms of aftershocks. Tectonophysics, 2021, 820, 229118.	2.2	9
9	Source Characteristics of the 2017 MsÂ6.6 (MwÂ6.3) Jinghe Earthquake in the Northeastern Tien Shan. Seismological Research Letters, 2020, 91, 745-757.	1.9	5
10	Joint Inversion of Geodetic Observations and Relative Weighting—The 1999 Mw 7.6 Chi-Chi Earthquake Revisited. Remote Sensing, 2020, 12, 3125.	4.0	2
11	The 2018 <i>M</i> _{<i>W</i>} 7.5 Papua New Guinea Earthquake: A Dissipative and Cascading Rupture Process. Geophysical Research Letters, 2020, 47, e2020GL089271.	4.0	18
12	Inelastic earthquake damage. Nature Geoscience, 2020, 13, 661-662.	12.9	3
13	Orthogonal Fault Rupture and Rapid Postseismic Deformation Following 2019 Ridgecrest, California, Earthquake Sequence Revealed From Geodetic Observations. Geophysical Research Letters, 2020, 47, e2019GL086888.	4.0	35
14	Source Characteristics of the 28 September 2018 Mw 7.4 Palu, Indonesia, Earthquake Derived from the Advanced Land Observation Satellite 2 Data. Remote Sensing, 2019, 11, 1999.	4.0	12
15	Confirmation of the double-asperity model for the 2016 MW 6.6 Akto earthquake (NW China) by seismic and InSAR data. Journal of Asian Earth Sciences, 2019, 184, 103998.	2.3	3
16	Cumulative and Coseismic (During the 2016 M w 6.6 Aketao Earthquake) Deformation of the Dextralâ€5lip Muji Fault, Northeastern Pamir Orogen. Tectonics, 2019, 38, 3975-3989.	2.8	12
17	Complex multiple-segment ruptures of the 28 September 2018, Sulawesi, Indonesia, earthquake. Science Bulletin, 2019, 64, 650-652.	9.0	12
18	Using Long-Term SAR Backscatter Data to Monitor Post-Fire Vegetation Recovery in Tundra Environment. Remote Sensing, 2019, 11, 2230.	4.0	19

Wanpeng Feng

#	Article	IF	CITATIONS
19	Source parameters of the 2017 <i>M</i> w 6.2 Yukon earthquake doublet inferred from coseismic GPS and ALOS-2 deformation measurements. Geophysical Journal International, 2019, 216, 1517-1528.	2.4	12
20	2017 MwÂ8.1 Tehuantepec Earthquake: Deep Slip and Rupture Directivity Enhance Ground Shaking but Weaken the Tsunami. Seismological Research Letters, 2018, 89, 1314-1322.	1.9	13
21	Source complexity of the 2016 <i>M</i> _W 7.8 Kaikoura (New Zealand) earthquake revealed from teleseismic and InSAR data. Earth and Planetary Physics, 2018, 2, 1-17.	1.1	7
22	Resolving Surface Displacements in Shenzhen of China from Time Series InSAR. Remote Sensing, 2018, 10, 1162.	4.0	26
23	Geodetic Constraints of the 2017 M _w 7.3 Sarpol Zahab, Iran Earthquake, and Its Implications on the Structure and Mechanics of the Northwest Zagros Thrustâ€Fold Belt. Geophysical Research Letters, 2018, 45, 6853-6861.	4.0	57
24	Source characteristics of the 2015 MW 7.8 Gorkha (Nepal) earthquake and its MW 7.2 aftershock from space geodesy. Tectonophysics, 2017, 712-713, 747-758.	2.2	43
25	Subsidence at Cerro Prieto Geothermal Field and postseismic slip along the Indiviso fault from 2011 to 2016 RADARSATâ€2 DInSAR time series analysis. Geophysical Research Letters, 2017, 44, 2716-2724.	4.0	16
26	Multidimensional Small Baseline Subset (MSBAS) for volcano monitoring in two dimensions: Opportunities and challenges. Case study Piton de la Fournaise volcano. Journal of Volcanology and Geothermal Research, 2017, 344, 121-138.	2.1	26
27	A Slip Gap of the 2016 <i>M</i> _w Â6.6 Muji, Xinjiang, China, Earthquake Inferred from Sentinelâ€I TOPS Interferometry. Seismological Research Letters, 2017, 88, 1054-1064.	1.9	38
28	Surface deformation associated with the 2015 Mw 8.3 Illapel earthquake revealed by satellite-based geodetic observations and its implications for the seismic cycle. Earth and Planetary Science Letters, 2017, 460, 222-233.	4.4	20
29	Significant lateral dip changes may have limited the scale of the 2015 <i>M</i> _{<i>w</i>} 7.8 Gorkha earthquake. Geophysical Research Letters, 2017, 44, 8847-8856.	4.0	22
30	MULTIDIMENSIONAL SMALL BASELINE SUBSET (MSBAS) FOR VOLCANO MONITORING IN TWO DIMENSIONS: OPPORTUNITIES AND CHALLENGES. CASE STUDY PITON DE LA FOURNAISE VOLCANO. , 2017, , .		0
31	An automated insar processing system: Potentials and challenges. , 2016, , .		10
32	Fast subsidence in downtown of Seattle observed with satellite radar. Remote Sensing Applications: Society and Environment, 2016, 4, 179-187.	1.5	12
33	The mechanism of partial rupture of a locked megathrust: The role of fault morphology. Geology, 2016, 44, 875-878.	4.4	83
34	Patterns and mechanisms of coseismic and postseismic slips of the 2011 M W 7.1 Van (Turkey) earthquake revealed by multi-platform synthetic aperture radar interferometry. Tectonophysics, 2014, 632, 188-198.	2.2	32
35	The 2011 MW 6.8 Burma earthquake: fault constraints provided by multiple SAR techniques. Geophysical Journal International, 2013, 195, 650-660.	2.4	71
36	The 2010 <i>M</i> _{<i>W</i>} 6.8 Yushu (Qinghai, China) earthquake: Constraints provided by InSAR and body wave seismology. Journal of Geophysical Research, 2011, 116, .	3.3	84

WANPENG FENG

#	Article	IF	CITATIONS
37	Using small baseline Interferometric SAR to map nonlinear ground motion: a case study in Northern Tibet. Journal of Applied Geodesy, 2009, 3, .	1.1	3
38	Spatio-temporal rupture process of the 2008 great Wenchuan earthquake. Science in China Series D: Earth Sciences, 2009, 52, 145-154.	0.9	156
39	Source process of M s6.4 earthquake in Ning'er, Yunnan in 2007. Science in China Series D: Earth Sciences, 2009, 52, 180-188.	0.9	13
40	The 1998 <i>M</i> _{<i>w</i>} 5.7 Zhangbei‣hangyi (China) earthquake revisited: A buried thrust fault revealed with interferometric synthetic aperture radar. Geochemistry, Geophysics, Geosystems, 2008, 9, .	2.5	24
41	The 2009 L'Aquila <italic>M</italic> _W 6.3 earthquake: a new technique to locate the hypocentre in the joint inversion of earthquake rupture process. Geophysical Journal International, 0, , .	2.4	16